Mini-magnetospheres and Moon-magnetosphere interactions: Overview Moon-magnetosphere Interactions

Joachim Saur

[1]Institut für Geophysik und Meteorologie, Universität zu Köln, Cologne, Germany

Key Points:

- Review of moon-magnetosphere interaction (MMI) in the solar system
- MMI is generally sub-Alfvénic and generates Alfvén wings with auroral footprints on planets
- Observations of MMI can reveal atmospheres, plumes, ionospheres, subsurface oceans, and dynamos

Corresponding author: Joachim Saur, `saur@geo.uni-koeln.de`

Abstract

"Moon-magnetosphere interaction" stands for the interaction of magnetospheric plasma with an orbiting moon. Observations and modeling of moon-magnetosphere interaction is a highly interesting area of space physics because it helps to better understand the basic physics of plasma flows in the universe and it provides geophysical information about the interior of the moons. Moon-magnetosphere interaction is caused by the flow of magnetospheric plasma relative to the orbital motions of the moons. The relative velocity is usually slower than the Alfvén velocity of the plasma around the moons. Thus the interaction generally forms Alfvén wings instead of bow shocks in front of the moons. The local interaction, i.e., the interaction within several moon radii, is controlled by properties of the atmospheres, ionospheres, surfaces, nearby dust-populations, the interiors of the moons as well as the properties of the magnetospheric plasma around the moons. The far-field interaction, i.e., the interaction further away than a few moon radii, is dominated by the magnetospheric plasma and the fields, but it still carries information about the properties of the moons. In this chapter we review the basic physics of moon-magnetosphere interaction. We also give a short tour through the solar system highlighting the important findings at the major moons.

1 Introduction

The outer planets of the solar system all possess large magnetospheres and harbor many natural satellites (for simplicity also called moons) within their magnetospheres. Thus the phenomenon of moon-magnetosphere interaction commonly occurs at the moons of Jupiter, Saturn, Uranus and Neptune and only rarely at Earth, when the Earth moon passes through the tail of its magnetosphere.

Moon-magnetosphere interaction is a sub-class of the interaction of a moving magnetized plasma with a celestial body. In terms of the very basic physics, there is no fundamental difference between a moon interacting with moving magnetospheric plasma or a planet interacting with the solar or a stellar wind or even an artificial satellite interacting with its plasma surroundings. In the solar system, however, under usual circumstances the relative velocities between the solar wind and the planets are larger than any of the three magneto-hydrodynamic (MHD) wave modes and bow shocks form. This is different in moon-magnetosphere interaction, where the relative velocities of the magnetospheric plasmas and the moons embedded within them are usually smaller than the wave velocity of the fast and Alfvén wave modes. Thus no bow shocks form around the moons. The interaction is sub-Alfvénic and so called Alfvén wings are being generated, which electromagnetically couple the moons and the planets.

1.1 Motivation

Why do we care to understand moon-magnetosphere interaction? Studying this interaction is important for two reasons: (a) The flow of plasma around an obstacle is a fundamental physical process of plasma, space and astrophysics and thus of basic interest. (b) The moons and their properties modify the plasma and magnetic field environment around the moons. Thus observations of the space environment around the moons through space probes and telescopes provide information about the properties of the moons which are often not accessible otherwise. Such plasma and magnetic field observation led, for example, to the discovery of plumes on Enceladus, and subsurface water oceans within Europa and Ganymede.

1.2 A short history

The progress of understanding moon-magnetosphere interaction is strongly tied to spacecraft missions to the outer solar system but it also has important contributions from

observations with telescopes. Moon-magnetosphere interaction was indeed first discovered remotely in Jupiter's radio emission, which contains a contribution that originates from Io's interaction with Jupiter's magnetosphere (Bigg, 1964). Io is historically the body with the best studied moon-magnetosphere interaction because it is the most powerful one in the solar system. The focus for decades remained with Io, where Pioneer 10 in the 1970s detected Io's ionosphere (Kliore et al., 1975), an important ingredient in its moon-magnetosphere interaction. The Voyager 1 and Voyager 2 spacecraft found that Io orbits within a dense plasma and neutral torus generated by mass loss from the moon (Broadfoot et al., 1979; Bridge et al., 1979). Voyager 1 made the first in-situ detection of moon-magnetosphere interaction when it passed south of Io (Acuña et al., 1981) and provided evidence for Io's Alfvén wings (Neubauer, 1980).

Observational evidence for moon-magnetosphere interaction at the other three Galilean satellites Europa, Ganymede and Callisto came with the Galileo mission to the Jupiter system beginning in 1995 with several close encounters at each of the moons (Kivelson et al., 2004). The Cassini spacecraft played the analogues role in the Saturn system starting 2004. It provided first observations of moon-magnetosphere interaction at the many inner icy moons of Saturn and visited its largest satellite Titan more than a 100 times.

Another milestone in remote sensing of the moon-magnetosphere interaction came through the discovery of so called auroral footprints of the moons. Again beginning with Io, observations in the infra-red (Connerney et al., 1993), followed by the UV, and the visible wavelength range, successively led to the detection of the footprints of Europa, Ganymede, Callisto and Enceladus so far (Clarke et al., 2002; Pryor et al., 2011; Bhattacharyya et al., 2018).

These observations sparked theoretical progress of the plasma-physical processes generated by the moons early on. Goldreich and Lynden-Bell (1969) developed for Io's interaction the so called unipolar inductor model, i.e., a steady-state electric current loop model. After the discovery of the dense Io torus, Neubauer (1980), Goertz (1980) and Southwood et al. (1980) however realized that basics of the interaction are best captured by considering the MHD waves generated by Io, which led to the family of Alfvén wing models. Further theoretical progress followed over the years where in addition to analytical descriptions, numerical simulations of the interaction nowadays play a very prominent role.

In this chapter we review basic principles of moon-magnetosphere interaction (Section 2). We classify the large variety of possible effects in subgroups (Section 3). Then we discuss the plasma physics of the interaction close to the moons and far away from them (Section 4). Finally we take a short tour to the moons in the solar system where moon-magnetosphere interaction occurs and we briefly look at extrasolar systems (Section 5). We end with a discussion of outstanding issues (Section 6). This chapter focuses primarily on large scale, i.e., MHD effects of the interaction. Due to the page limit we discuss kinetic effects to a smaller extent and we omit moon-radiation belt interactions. The latter have led among other things to the discovery of a few small moons and can be considered a special case of the high energy tail of the plasma-moon interaction.

2 Basic setup

In Figure 1 we show the basic setup of moon-magnetosphere interaction, where the Jupiter system is used as an example. The moons are embedded within the closed magnetospheric field lines of the central planet and revolve about the planets with Keplerian velocities (see orange lines in Figure 1). Their orbital periods are on the order of days to tens of days. The magnetospheric plasmas are frozen into the magnetospheric fields and partly corotate with the planets, which have rotation periods on the order of tens of hours. Due to an incomplete coupling to the planets' ionosphere, the magneto-
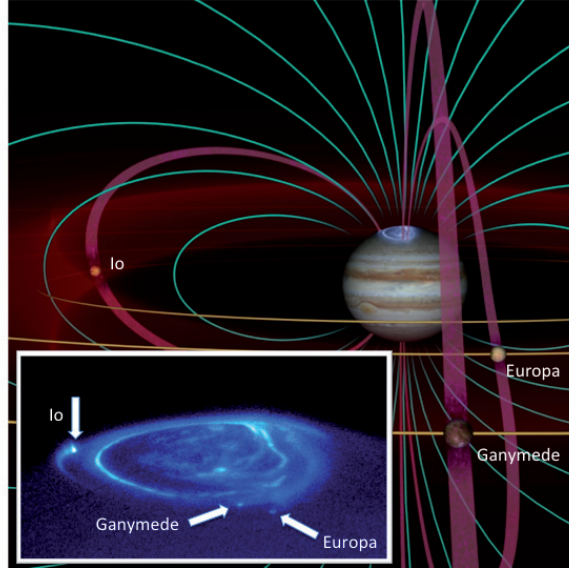
Figure 1. Set up of moon-magnetosphere interaction for the case of Jupiter's Galilean moons. The blue inlet is a zoom into Jupiters polar region and displays Jupiter's main aurora and the auroral footprints of the moons Io, Europa, and Ganymede. Turquoise lines represent Jupiter's magnetic field lines, and the orange lines show the orbits of the moons. The pink flux tubes display field lines connecting the moons with Jupiter. Electric currents and energy generated by the moon interaction is being transported along these flux tubes. Where the flux tubes intersect with Jupiter's atmosphere, auroral emission is excited. The plasma generated by Io produces a torus around Jupiter (shown in orange/red). The radial transport of this plasma generates magnetic stresses and electric currents (not shown), which couple to Jupiter and generate its main auroral oval. (Image Credit: John Spencer and John Clarke).

spheric plasma is only partly corotating with the planet, which is referred to as "sub-corotation". The resulting azimuthal velocities of the subcorotating plasma at the orbital distances of the moon is however still much larger than the orbital velocities of the moons, which results in a relative velocity between the magnetospheric plasma and the moons. In other words, the moons are constantly overtaken by the magnetospheric plasma.

Therefore the moons are obstacles to the flow of magnetospheric plasma and thus perturb the plasma and magnetic field environment around them. This interaction generates waves, which propagate away from the moons. The most important wave is the Alfvén mode, whose group velocity in the rest frame of the plasma travels strictly parallel and anti-parallel to the ambient magnetic field. In the rest frame of the moon, this leads to standing Alfvén waves, called Alfvén wings. Where these wings intersect with the planets' atmosphere/ionosphere auroral emission is generated, which is referred to as footprints of the moons (see Figure 1).

3 Classification of interactions

Now we study how the various interactions at the moons in the solar system can be classified. Starting from the general case of the interaction of planetary bodies within any type of moving magnetized plasma, we subdivide the interaction into several subclasses. Two basic criterion to categorize the interaction are (a) the properties of the external plasma which the moon is exposed to and (b) the properties of the moon. We will

systematically discuss these properties in the next two subsections. An additional criterion is the nature of the coupling between the moon and the host planet, which we subsequently present in Section 3.3.

3.1 Properties of the magnetospheric plasma

In most cases moon-magnetosphere interaction can be described within the magnetohydrodynamic (MHD) framework. MHD is applicable if the ion gyroradius of the plasma is significantly smaller than the spatial scales of the moons and if the ion gyroperiod is significantly smaller than typical time scales, e.g., the convection time of the plasma past the moon. In nearly all the cases of moon-magnetosphere interaction, this is a very good assumption. We will discuss some exceptions and modification of moon-magnetosphere interaction through non-MHD effects in Section 5.

The MHD wave modes, i.e., the shear Alfvén mode, the magneto-acoustic modes and the convecting entropy mode play the most important role in the interaction. Basic properties of these modes are given by the Alfvén velocity v_A and the sound velocity c_s, which lead to the Alfvén Mach number

$$M_A = \frac{v_0}{v_A} \qquad \text{with} \quad v_A = B/\sqrt{\mu_0 \rho} \,, \tag{1}$$

the sonic Mach number

$$M_S = \frac{v_0}{c_s} \qquad \text{with} \quad c_s = \sqrt{\gamma p/\rho} \,, \tag{2}$$

and the fast Mach number

$$M_f = \frac{v_0}{\sqrt{c_s^2 + v_A^2}} = \frac{1}{\sqrt{\frac{1}{M_s^2} + \frac{1}{M_A^2}}} \tag{3}$$

with the relative velocity between the magnetospheric plasma and the moon v_0, the magnetic field strength B, the plasma mass density ρ, the total plasma pressure p, i.e. the sum of the ion and electron thermal pressure and the adiabatic exponent $\gamma = 5/3$. The definition of the Mach numbers directly imply $M_f \leq M_A$ and $M_f \leq M_S$. The Alfvén and sound speeds also constrain the plasma β, i.e., the ratio between the thermal and the magnetic pressure given by

$$\beta = \frac{p}{B^2/2\mu_0} = \frac{2}{\gamma} \left(\frac{M_A}{M_s} \right)^2 \,. \tag{4}$$

The most important classification criterion is whether the fast Mach number $M_f \gtrsim 1$. Then waves excited by the moon cannot propagate upstream because the flow velocity is larger than the largest wave speed. In this case a bow shock forms. In nearly all the cases of moons in planetary magnetospheres the Alfvén Mach number obeys $M_A < 1$, thus $M_f < 1$ as well, and no bow shock in front of the moon develops. This type of interaction is referred to as sub-Alfvénic interaction. The most prominent exception can be Titan and possibly Callisto.

Another important criterion is the plasma beta. In case of sub-Alfvénic interaction, low plasma beta $\beta \ll 1$ implies the interaction is controlled by the magnetic energy of the magnetospheric plasma. This generates a "stiff" magnetic field environment. In case of large plasma beta $\beta \gg 1$, the thermal energy of the plasma dominates the interaction. In this case, the magnetic field lines are strongly draped around the obstacle because the thermal pressure dominates the flow around the obstacles and takes the magnetic field via the frozen-in-field theorem with it.

3.2 Properties of the moons (atmosphere, ionosphere, dynamo, oceans)

The various properties of the moons influence their space environment as well. The primary root cause of the interaction is that the moons act as obstacles and modify the flow of plasma around them through mechanical or electromagnetic forces.

3.2.1 Mechanical Obstacles

Mechanical obstacles are the solid surfaces of the moons, which absorb the plasma on the upstream side and which generate wakes of void plasma on the downstream side. The moons' atmospheres and exospheres including dust are also mechanical obstacles because collisions with the plasma and ionization cause a modification of the velocity and momentum of the plasma. Collisions can pertain to elastic collisions or charge-exchange collisions. Ionization of neutrals leads to fresh ions and electrons, which are subsequently reaccelerated by the ambient motional electric fields. This processes is refereed to as pickup (Vasyliūnas, 2016). The effects of collisions and ionization can be formally combined to 'effective collision frequencies' used in the electron and ion equations (Neubauer, 1998). Collisions and pickup both cause the electrical conductivities in the moons ionospheres.

3.2.2 Electromagnetic Obstacles

Moons with an intrinsic magnetic field interact electromagnetically with the surrounding plasma. The intrinsic magnetic fields can be due to an internal dynamo field, such as within Ganymede (Kivelson, Khurana, Russell, et al., 1996). Other possibilities are induced magnetic fields in the interior. Time-variable external magnetic fields generate secondary magnetic fields within electrical conductive layers such as internal saline water oceans. Those secondary fields modify the magnetic field and plasma flow around the moons (Khurana et al., 1998; Neubauer, 1998; Schilling et al., 2007).

3.3 Unipolar inductor vs Alfvén wing model

Moon-magnetosphere interactions generate Alfvén waves, which travel along the host planets moving magnetospheric field lines and eventually hit the planet. Where the Alfvén waves intersect with the atmosphere and ionosphere of the planet auroral emission is being observed (Connerney et al., 1993). The Alfvén waves are partially reflected at the planet's ionosphere and travel back towards the moon. When the reflected wave misses the moon because the magnetospheric plasma has traveled far enough downstream, then no feedback coupling between the moon and planet is possible. This case is called the pure Alfvén wing model. It occurs when the wave travel time from the moon to the planet and back $2\tau_{\mathrm{wave}}$ is larger than the convection time of the plasma past the moon τ_{conv} (Neubauer, 1980, 1998). If the wave travel time is much shorter than the convection time, then a force balanced situation with only field-aligned currents between the moon and the planet is reached, which is referred to as the 'unipolar inductor case' (Goldreich & Lynden-Bell, 1969). The situation where the waves can only partially couple back, can be referred to as the mixed Alfvén wing case (Neubauer, 1998).

4 Physics of the interaction

The physics and the effects of moon-magnetosphere interaction can be conveniently divided into the physics of the local interaction, i.e., within several radii of the moon. In this region the detailed nature of the obstacle plays an important role in controlling the space environment around the moons. The regions further away is often referred to as far-field. It includes for example the Alfvén wings, the auroral footprints and their tails.

4.1 Physics of the local interaction (i.e., within several moon radii)

The root cause of the interaction occurs in the local interaction. Mechanical or electromagnetic forces slow and modify the magnetospheric plasma flow. The locally modified flow generates magnetic field perturbations and also leads to MHD and other wave modes. The local interaction is generally very complex because the different wave modes interact non-linearly. In the local interaction the detailed aeronomic processes that occur in the atmospheres and exospheres need to be considered as well.

In the following we mostly discuss cases of moon-magnetosphere interaction where at the surface of the moon the magnetospheric field of the central planet is larger than the magnitude of the internal magnetic field. In this way, no closed magnetic field lines region around the moons develop. The only known moon with closed field lines is Ganymede (Kivelson, Khurana, Russell, et al., 1996; Neubauer, 1998; Jia et al., 2008; Duling et al., 2014). Ganymede's space plasma environment is reviewed in a separate chapter by X. Jia et al.

4.1.1 Plasma flow in the atmosphere and magnetic draping

In Figure 2 we sketch the local interaction in the sub-Alfvénic case for (a) low plasma
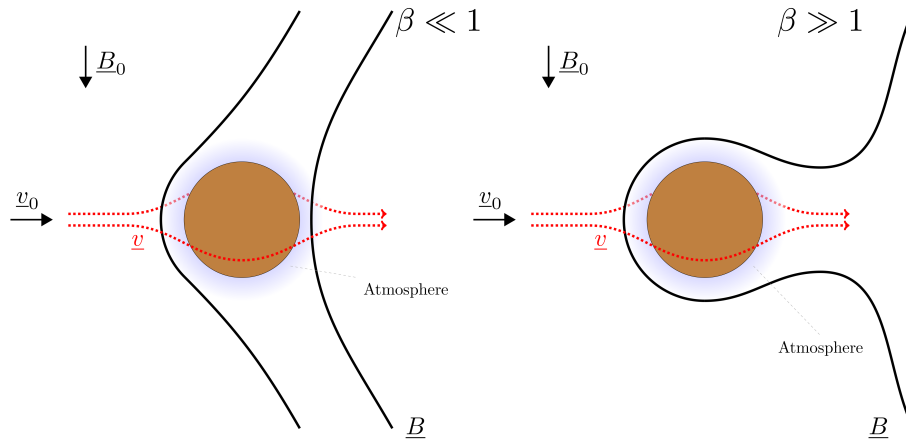

Figure 2. Sketch of local plasma interaction in the sub-Alfvénic case for (a) low plasma beta $\beta \ll 1$ and (b) high plasma beta $\beta > 1$.

$\beta \ll 1$, e.g., Io's environment, and (b) for high plasma $\beta > 1$, e.g., Titan's environment. In both cases charge-exchange and collisions between magnetospheric ions and atmospheric neutral particles strongly slow the initially fast moving plasma. Pickup, i.e., ionization of the neutrals, which move with very slow velocities in the rest frame of the moons, adds new slow-moving plasma to the magnetospheric plasma and thus slows the total plasma as well.

The slowed plasma flow causes a change in the surrounding magnetic field. The plasma outside of a moon's atmosphere obeys the frozen-in-field theorem. The flow outside of the atmosphere is generally much faster compared to the flow in the atmosphere which leads to draped magnetic field lines around the moons. On the flanks of the moons, the velocity can be accelerated to velocities up to twice the upstream velocity v_0 (Saur, 2004). The draping is particularly strong in cases of large plasma beta and much weaker for low plasma beta (see Figure 2). The reason is that in the low beta case, the energy density in the magnetic field dominates the thermal energy density. This is often the case for

moons which are closer to the planets. For low plasma betas, the strong background magnetic field acts as a stiff magnetic field, which controls the topology of the field. It results in larger magnetic tension forces compared to the pressure gradient, which prevents the draping. Next to the magnetic field direction the field magnitude is also modified in the interaction. On the upstream side the magnetic field strength is enhanced due to compressional effects, which is referred to as magnetic pileup, while on the downstream side the field magnitude is decreased compared to the unperturbed magnetic field.

4.1.2 Aeronomy and formation of ionospheres

Even though the main engine of moon-magnetosphere interaction is the momentum exchange between the magnetospheric plasma and the moon, the detailed processes in the moons' atmospheres and ionospheres are often controlled by complex aeronomic processes. The two main ionization processes in the moons' atmospheres are electron impact ionization and photo-ionization. Electron impact ionization can occur through the thermal and non-thermal electrons in the planets' magnetospheres. Energetic electrons produced by the interactions can additionally contribute to ionization. This can be electron beams generated within the Alfvén wings, which return to the moon and generate a feedback loop within the interaction (Williams et al., 1996; Jacobsen et al., 2010). At Ganymede the interaction drives additional sources of energetic electrons in form of reconnection and wave particle interaction within and near the closed field line region of Ganymede's magnetosphere (Williams et al., 1997; Eviatar et al., 2001). The ionospheres are often not in chemical equilibrium, i.e., ionization is not balanced by recombination, but additionally controlled by convection of ionospheric plasma. Convection thus plays an important role in shaping the spatial structures of the moons ionospheres. Electron impact ionization rate depends on the neutral and electron density, but also highly nonlinearly on the electron temperature or its distribution function (Rees, 1989).

4.1.3 Interaction strength and ionospheric Pedersen and Hall conductances

The presence of a magnetic field makes the electrical conductivity of a plasma anisotropic. Within the ionospheres of the moons, the conductivity tensor is conveniently separated in Birkeland conductivities σ_B (parallel to the magnetic field), in Pedersen conductivities σ_P (perpendicular to the magnetic field, but still along the electric field), and the Hall conductivities σ_H (perpendicular to the magnetic and electric field). Except for the case of Titan, the Birkeland conductivities can be considered nearly infinite within the moon's ionospheres (Neubauer, 1998) which leads to negligible field aligned electric fields in the ionospheres. Therefore the Pedersen and Hall conductivities can be integrated along the field lines to obtain height-integrated conductivities, referred to as Pedersen and Hall conductances, Σ_P and Σ_H, respectively. The values and the spatial structure of these conductances strongly constrain the ion and electron flow in the moons' ionospheres.

The conductances can be used to characterize the strength of the moon-magnetosphere interaction. The interaction strength $\bar{\alpha}$ quantifies how strongly the magnetospheric flow is reduced within the moons' ionospheres (Saur et al., 2013). It is defined by

$$\bar{\alpha} \equiv \frac{\delta v}{v_0} \approx \frac{1}{M_A}\frac{\delta B}{B_0} \tag{5}$$

with $\delta v = |v - v_0|$ and $\delta B = |B - B_0|$ the amplitudes of the velocity and the magnetic field perturbations in the Alfvén wings or approximately in the vicinity of the moons. The interaction strength varies between zero and its maximum value one, when the plasma flow comes to a halt near the moons, i.e., $v = 0$. In case of an Alfvénic far-field interaction, the interaction strength can be approximated as $\bar{\alpha} = \Sigma_P/(\Sigma_P + 2\Sigma_A)$ or by the ratios of the moon's ionospheric conductances to those of the planet in case of the unipolar inductor far-field interaction (Goldreich & Lynden-Bell, 1969; Saur, 2004).

The ionospheric Hall effect breaks the interaction symmetry and rotates the flow and the magnetic field. The ionospheric electric field and the electron flow are rotated by the angle $\Theta_{\text{twist}} = -\Sigma_H/(\Sigma_P + 2\Sigma_A)$ (Saur et al., 1999). The magnetic field perturbations in the Alfvén wings are rotated by the same angle. At the presence of a significant dust component in the plasma, a fraction of the electrons might be attached to the mostly immobile dust grains. Accordingly ions are not the most massive charge carrier in the plasma anymore. This can generate an anti-Hall effect with reversed sign of the Hall conductances and thus reversed directions of the electron flow and fields as observed within the plumes of Enceladus (Simon, Saur, Kriegel, et al., 2011; Kriegel et al., 2011).

4.1.4 Overall energy fluxes

It is interesting to look at the overall partioning of the energy fluxes in moon magnetosphere interactions. For simplicity we only consider the low Alfvén Mach number $M_A \ll 1$ and the low plasma beta case $\beta \ll 1$ under the assumption that the unperturbed plasma velocity v_0 and magnetic field B_0 are perpendicular. The largest energy flux, which the moon's atmosphere/ionosphere system is exposed to, is the Poynting flux of the magnetospheric plasma, i.e., the bodily transport of magnetic enthalpy. Assuming the ionospheric obstacle has a radius of R, then the Poynting flux of the upstream flow is $S_{in} = \pi R^2 E_0 B_0/\mu_0$ with the motional electric field $E_0 = v_0 B_0$. The energy dissipated as Joule heating in the moons' ionospheres can be approximated by $P = 4\pi \,\bar{\alpha}(1-\bar{\alpha})M_A R^2 E_0 B_0/\mu_0$ (Neubauer, 1980). The Joule dissipation P is maximum for intermediate interaction strength $\bar{\alpha} = 1/2$. The total energy radiated away within both Alfvén wings towards the planet is $S_A = 4\pi \,\bar{\alpha}^2 M_A R^2 E_0 B_0/\mu_0$ (Saur et al., 2013). The ratio $S_A/P = \bar{\alpha}/(1 - \bar{\alpha})$ depends only on the interaction strength $\bar{\alpha}$. The Alfvénic Poynting S_A flux is larger than the ionospheric Joule dissipation for $\bar{\alpha} > 1/2$ and S_A assumes its maximum if the interaction strength is maximum, i.e. $\bar{\alpha} = 1$. How much of the Alfvénic Poynting flux in the wings directly enters and heats the planets' ionospheres strongly depends on the nature of the far-field coupling (Goldreich & Lynden-Bell, 1969; Neubauer, 1998).

4.1.5 Induction in the interiors: Diagnosing saline oceans

Time-variable magnetic fields outside of the moons induce electric fields according to Faraday's law of induction. Any electrically conductive layers will then generate electric currents which produce secondary magnetic, i.e., induced magnetic field. In case of Jupiter, Uranus and Neptune, the magnetospheric fields in the rest frame of the moons are quasi-periodic due to the tilt of the magnetic moments of the planets with respect to their spin axis. Observations of induced magnetic fields outside of the moon are thus diagnostic of electrical conductive layers (Khurana et al., 1998; Kivelson et al., 2000; Zimmer et al., 2000). This method is a very powerful tool to detect currently liquid, electrically conducting oceans under the icy crust of some of the moons, in particular Europa and Ganymede. The method is based on the fact that the electrically conductivity of a mantle composed of pure ice and rock compared to a saline ocean as expected for these icy satellites is several orders of magnitudes smaller and would not produce observable magnetic fields (Khurana et al., 1998).

For a quantitative analysis of the induction effects, both the inducing and the induced fields need to be known. Therefore in general two satellites which measure both fields separately are necessary. In case of quasi-periodic fields, the inducing fields from magnetospheric measurements (often combined with theoretical models) can be used such that single flybys at the moons are sufficient. However attention still need to be paid to separate magnetic fields generated by internal induction from other sources of magnetic field perturbations, e.g., due to the plasma interaction with the atmosphere (Schilling et al., 2007, 2008).

In case the inducing magnetospheric fields at the moon can be considered spatially constant over the size of the moon, which is usually a very good assumption, and under the assumption of a radially symmetric conductivity distribution, the induced field is a dipole magnetic field outside of the moon (Zimmer et al., 2000). Thus observations of a dipole field perturbation with the appropriate phase with respect to the inducing field allows to derive constraints on electrically conductive layers.

The induction sounding technique is non-unique. Observations of one single inducing frequency does not allow to separate thickness and conductivity of the electrically conductive layer, but only approximately constrain the product of both (Zimmer et al., 2000; Seufert et al., 2011). The analysis of magnetic field measurements obtained during multiple flybys or from an orbiter around the moons is thus a powerful tool to probe various inducing frequencies and thus to disentangle various subsurface ocean properties (Khurana et al., 2002; Seufert et al., 2011) (as planned for the Europa Clipper and the Juice Missions).

4.1.6 Induction in the ionospheres

In addition to induction in the interior of the moons, time-variable magnetic fields can also generate induced fields in the electrically conductive ionospheres of the moons. The conductivity in an ionosphere is anisotropic (see Section 4.1.3). In saline oceans or in electronically conductive metals and rocks the conductivity is however approximately isotropic. Recently it was shown that induction in an ionosphere is controlled by an effective conductance $\Sigma_{\mathrm{eff}} = \Sigma_P + \Sigma_H^2/(\Sigma_P + \Sigma_A)$ (Hartkorn & Saur, 2017). In case of large Hall conductances Σ_H and small Alfvén conductances, a significant enhancement effect occurs compared to the individual Hall and Pedersen conductances. The underlying process is similar to the Cowling channel effects known from the Earth's ionosphere (Cowling, 1932; Baumjohann & Treumann, 2012). Because the ionospheric conductivities depend on the neutral and the ion densities and are inversely-dependent on the magnetic field strength, ionospheres with large densities or moons at large orbital distances within smaller magnetospheric fields have large effective conductances and will thus generate sufficiently strong induced fields. In the case of Callisto, the effective ionospheric conductances can be as large as the ocean conductances (Hartkorn & Saur, 2017). Thus observations of induced fields do not necessarily imply the existence of a subsurface oceans. Thus observations of induced fields at distances significantly above the ionosphere do not necessarily imply the existence of a subsurface ocean. Observations, which better constrain the spatial distribution of Callisto's ionospheric and neutral densities are necessary to better quantify the ionospheric contribution to induction, particularly on the night side. If possible, flybys below the peak of the ionospheric densities would help disentangle induction effects in ionospheric and internal layers.

4.1.7 Wakes, upstream-down stream asymmetries

Moon-magnetosphere interactions possess a pronounced upstream-downstream asymmetry (see also section 4.1.1). Compared to hydrodynamic flows around solid objects, the flow of plasma onto moons with very dilute atmospheres leads to absorption of plasma on the surfaces of the upstream side. This effect causes the formation of a wake of void plasma on the downstream side. The void plasma wake will be partially filled by plasma driven by thermal pressure. In case of low Alfvén Mach number M_A and small plasma beta, the plasma will move along the magnetic field lines at a rate increasing with the sonic Mach number M_S (Neubauer, 1998). The rarefied plasma in the wake leads to a reduced thermal pressure compared to plasma on streamlines without absorbed plasma. The resultant pressure gradients into the wakes are partially compensated by enhanced magnetic pressure associated with diamagnetic currents. The wake effects will thus lead to enhanced magnetic field magnitudes in the wakes. These perturbations have been observed and modeled initially at the Earth's moon (Whang, 1968) and subsequently stud-

ied for example also at the nearly inert moons Tethys and Rhea (Khurana et al., 2008; Simon et al., 2009, 2012). In the case of Io, it can explain the double-peaked magnetic field structure in its wake (Saur et al., 1999).

When strong mass-loading in the moons' atmospheres or exospheres occurs, in particular on the flanks, the new plasma is transported downstream and produces another part of the wake with enhanced density outside of the rarefied wake. This density will generate a density wave along the magnetic field lines (Schilling et al., 2008).

4.1.8 North-South asymmetries

Asymmetries in the moons' neutral gas environment will generate asymmetries in the moon-magnetospheric interaction. Let us assume for simplicity that the background magnetic field is in the north-south direction. An atmospheric asymmetry between the north and the south, for instance, due to the plumes on Enceladus, will drive different ionospheric electric currents in the north and the south. With the exception of Titan with its dense atmosphere, field lines which pass the moons' atmospheres, but which do not penetrate the solid body of the moons, are equipotentials due to very large field-aligned conductivity σ_B within the thin atmospheres of the moons (Neubauer, 1998). Because the solid surfaces of the moons are electrically insulating, magnetic field lines which penetrate the surface do not need to be equipotentials anymore. In case of an atmospheric north-south asymmetry, different amounts of electric currents are driven in both hemispheres which are continued along the magnetic field lines in the northern and southern magnetosphere, respectively. The asymmetric amount of electric current between both hemispheres is partially reduced by hemispheric currents, which connect both hemispheres (Saur et al., 2007). These hemisphere currents generate rotational magnetic field discontinuities on field lines tangent to the solid body of the moons. Such discontinuities have been identified in the magnetic field environment of Enceladus (Simon et al., 2014). The hemisphere currents and discontinuities are suited to search for plumes and atmospheric asymmetries, but they are less pronounced in case a globally symmetric atmosphere is present (Blöcker et al., 2016).

4.1.9 Non-MHD effects

Most of the large scale features of moon-magnetosphere interactions can be described by resistive single fluid MHD when the ionospheric Hall effect is included. Several of the following multi-fluid or non-MHD effects can however be important as well: (1) In case the ion population cannot be appropriately modeled with one effective ion, multi-ion fluid effects need to be considered (Paty & Winglee, 2004; Ma et al., 2006). (2) In some cases, it is important to consider the electron physics separately. For example, electron heat conduction can maintain ionospheric electron temperatures at a level such that electron impact ionization is the dominant ionization source (Saur et al., 1998; Backes et al., 2005; Rubin et al., 2015). (3) In case photoionization is the dominant ionization source, strongly non-Gaussian electron distribution functions can arise, which require a kinetic, i.e. Vlasow-based description, e.g., at Titan and Callisto (Vigren et al., 2016; Hartkorn et al., 2017). (4) Due to the decreasing planetary magnetic field strength with distance from the planet, large gyroradii-effects can play a role at some of the moons. When ions are picked up on the flanks of the moons where the convection velocity is large, gyroradii as large as the moons can occur. (Kivelson et al., 2004; Liuzzo et al., 2015). Prominent examples are Titan and Callisto. However, a large fraction of the pickup ions at these moons have still small gyroradii because the ionization occurs within the bulk atmosphere where the plasma flow is significantly slowed (Hartkorn & Saur, 2017). (5) For the total plasma pressure, the suprathermal ions can play an important role. At Jupiter's Galilean moons, the pressure of the suprathermal magnetospheric ions can be comparable or larger than the thermal ion pressure (Mauk et al., 2004) (6) Reconnection and particle acceleration

processes at Ganymede's magnetosphere are strongly controlled by kinetic ion and electron physics (Tóth et al., 2016).

4.2 Physics of the far-field interaction: Alfvén wings and footprints

The far-field interaction is the region starting several moon radii away from the moons. It does not include the moons' ionospheres any more. The far-field is strongly controlled by the MHD wave modes. The transition from the local interaction into the far-field is included in all standard 3D numerical models and continuation of electric current from the local interaction into the Alfvén wings is usually included in the analytic models as well.

4.2.1 Role of MHD waves

Let us look at the far-field effects at various limits. For simplicity we first assume that the magnetospheric fields are spatially and temporally constant and the interaction is sub-Alfvénic. In the limit of negligible plasma pressure, i.e., the approximately zero plasma-beta, the propagating wave modes are the fast mode and the Alfvén mode. The fast mode is in this case isotropic in the plasma rest frame. Therefore the energy flux density of the fast mode decreases with distance squared. Thus the fast mode amplitudes are negligible at sufficiently large distances from the moons. The Alfvén mode, in contrast, has a fully anisotropic group velocity, which is strictly parallel or anti-parallel to the background magnetic field in the rest frame of the unperturbed plasma. The Alfvén mode is therefore the most important mode in the far-field because the wave energy density does not decrease along the path of its group velocity. The Alfvén mode can be conveniently described in Elsässer variables (Elsässer, 1950), which are also the characteristics of the equations. They are given by

$$\mathbf{z}^{\pm} = \mathbf{v} \pm \frac{\mathbf{B}}{\sqrt{\mu_0 \rho}} \ . \tag{6}$$

In case of a north south orientation of the magnetospheric field at the location of the moon (like at Jupiter or Saturn), the $\mathbf{z}^{+}$ variable characterizes the southern Alfvén wing and $\mathbf{z}^{-}$ the northern wing. The wings are inclined with respect to the background magnetic field by an angle $\tan^{-1} M_A$ (Neubauer, 1980). The reason is that while the wave propagates along $\mathbf{B_0}$ it is simultaneously convected downstream by $\mathbf{v_0}$. In case that the north and south propagating waves do not intersect and the background fields are constant, an Elsässer variable being constant constitutes an exact solution of the non-linear incompressible MHD equations. This is an important fact because it describes that non-intersecting Alfvén waves can propagate without dispersion and dissipation towards the central planet.

In Figure 3 we display the basic magnetic field and velocity structure in an Alfvén wing. Velocity streamlines are shown in green and magnetic field lines are in red and orange. In the center of the main Alfvén wing (shown as purple tube) the flow is slowed. This results from the slowed flow in the moons' atmospheres, which is caused by collisions of the plasma with the atmospheric neutrals and by pickup due to ionization of neutrals. The slowed plasma flow in the atmospheres is then propagated as Alfvénic velocity and associated magnetic field fluctuations into the Alfvén wing. Within the Alfvén wing the streamlines have a significant component parallel to the characteristic and thus follow the wing over a certain distance. In case of maximum interaction strength, i.e., $\bar{\alpha} = 1$, the flow within the main wing would only have a component parallel to the tube and thus would stay within it. Outside of the main wing, the flow is directed around the region of slowed plasma with increased velocities on the flanks to maintain incompressibility. The magnetic field lines within the main wing (in red) are bend back compared to the background magnetic field and follow the tube. In the case of $\bar{\alpha} = 1$, the magnetic field in the main wing would be perfectly parallel to the wing and magnetic field lines would stay within it as well. In all other cases $\bar{\alpha} < 1$, the magnetic field lines re-
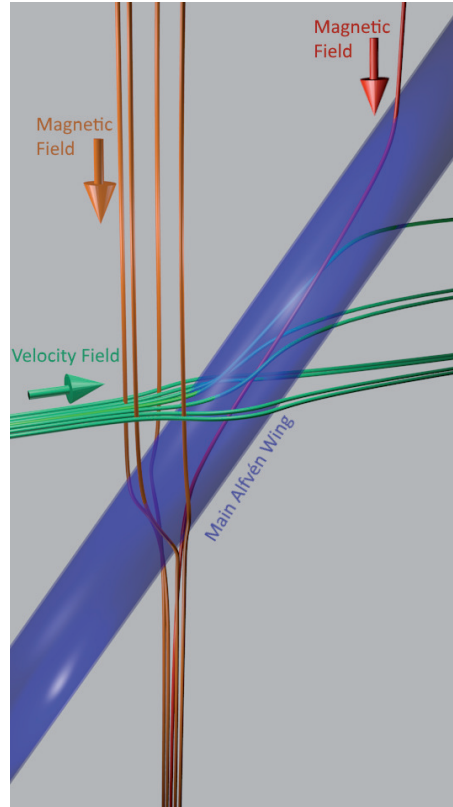
Figure 3. Magnetic field lines (orange and red) and velocity stream lines (green) within an Alfvén wing. Field lines in red pass through the main wing and the field lines in orange pass outside of the main wing. The purple tube characterizes the boundary of the main wing which corresponds to the size of the source, i.e., the moon. Inside the main wing the magnetic field lines are bent towards the direction of the tube, i.e., in downstream direction, outside of the main wing on the flanks the magnetic field lines are bent in the opposite direction, i.e., upstream.

side within the main wing for a certain distance and then turn towards the unperturbed direction. Outside of the main wing on their flanks, the magnetic field lines (in orange) are bent in the opposite direction compared to the direction of the bent within the wing. The resulting magnetic stresses are such that they are balanced by acceleration or deceleration of the plasma.

Around the moons and partly within the Alfvén wing the slow mode plays an important role as well. The propagation of the slow mode strongly depends on the plasma temperature. If the sound speed is much slower than the Alfvén velocity, i.e. $\beta \ll 1$, the slow mode propagates primarily along the magnetic field with a slow mode wing inclined by $\tan^{-1} M_S$. A sonic shock then propagates strictly along the magnetic field. If the sound speed is larger than the Alfvén velocity, the sonic mode propagates with the Alfvén velocity. The resultant wing contains Alfvénic and slow mode features. It is fan-shaped in the plane containing the background velocity and the magnetic field. The structure is also referred to as delta wing and has an opening angle of approx $\tan^{-1} M_A$ (Neubauer et al., 2006).

4.2.2 Kinetic effects in far-field

A part of the far-field interaction is not controlled by ordinary MHD. Kinetic effects are responsible for the acceleration of particles which generate the footprints of the moons in Jupiter's atmosphere through the electromagnetic wavelengths spectrum (Connerney et al., 1993; Prangé et al., 1996; Clarke et al., 1996; Pryor et al., 2011) and for the radio-emission generated along the Alfvén wings (Bigg, 1964; Zarka, 1998; Zarka et al., 2018; Louis et al., 2017). Due to the strong magnetic field and the small plasma densities in this region, the displacement current in Ampére's law needs to be included and for electron energies larger than a few 100 keV the relativistic mass of the electrons need to be considered.

Theoretical ideas for the particle acceleration mechanisms have been developed primarily for Io's Alfvén wings and are mostly based on the filamentation of the main wing (Chust et al., 2005). These filamented Alfvén waves are suggested to turn into kinetic Alfvén waves and develop stochastic magnetic field aligned electric fields, which can generate broad band electron distributions (Hess et al., 2010; Hess et al., 2011; Hess & Delamere, 2013; Saur et al., 2018). The resultant electron beams can trigger the electron maser instability, which causes the satellites' controlled radio emission (Bigg, 1964; Zarka, 1998; Zarka et al., 2001; Zarka, 2007; Zarka et al., 2018). Su et al. (2002) investigated electron acceleration downstream of the main wing with a steady-state Vlasov model by applying a potential drop. Alternatively, Crary (1997) suggested that repeated Fermi-acceleration can generate Io's electron beams.

5 Short tour of moons in magnetospheres: Earth, Jupiter, Saturn, Uranus, Neptune, and Exoplanets

Now we take a very short tour to the moons located within the respective magnetospheres of their host planets. Because of the very large number of moons in the solar system, we can only cover a selected number of moons guided by scientific interest and size. Thus we do not cover moons associated with planets or dwarf planets with at most only weak internal magnetic fields like Mars and Pluto. We include Earth's moon even though it is only a fraction of the time in the magnetosphere. In case of Jupiter we cover the Galilean moons, in case of Saturn the larger inner icy moons plus Titan, in case of Uranus and Neptune we consider all moons with diameters larger than 1000 km. These objects, their main properties and associated references are listed in table 1.

5.1 Earth: Moon

The Earth's moon orbits our planet with a semi-major axis of 60.3 R_E (Earth radii). The Earth magnetopause on the sub-solar side is located at roughly 10 R_E. Thus the moon is mostly located in the solar wind and thus subject to a super-fast $M_f > 1$ flow, but spends 20 % of its orbit in the terrestrial magnetosphere (Harnett et al., 2013). During its magnetospheric phase, the moon is subject to strongly varying properties from nearly vaccum-like densities in the magnetospheric lobes to the plasma sheet, in which number density and heavy ion concentration can change on rapid time scales (Harnett et al., 2013). Since the moon possesses only a very dilute exosphere, it acts mostly as an inert obstacle to the flow but moon originating ions are still observed in the Earth's magnetosphere. These studies date back to the sixties with more recent work published by, e.g., Tanaka et al. (2009) and Halekas et al. (2012).

5.2 Jupiter: Io, Europa, Ganymede, Callisto

Jupiter possesses four large moons orbiting permanently within its magnetosphere: Io, Europa, Ganymede and Callisto (Table 1). As mentioned in Section 1, Io's interaction is historically the best studied moon-magnetosphere interaction likely because it is

Table 1. Overview of moon-magnetosphere interaction properties for selected solar system moons. Table includes: Radius, semi-major axis, magnetospheric field strength B_0 at location of moons, relative velocity v_0 between moons and magnetospheric plasma, magnetospheric plasma density n_p at location of moon, Alfvén Mach number M_A, sonic Mach number M_S, plasma β and interaction strength $\bar\alpha$, comments, and references. (1): Spice Library (Acton, 1996), (2): Spice Library and values in units of volume mean radii R_P for Earth: 6371.01 km, Jupiter: 69911 km, Saturn 58232 km, Uranus: 25362 km, Neptune: 24624 km (Acton, 1996), (3): Halekas et al. (2012), Harnett et al. (2013), (4): Kivelson et al. (2004), (5): Kivelson et al. (2004), Khurana et al. (1998), Saur et al. (1998) (6): Kivelson et al. (2004), (7): Kivelson et al. (2004), Strobel et al. (2002), Hartkorn and Saur (2017), (8): Saur (2005), (9): Dougherty et al. (2006), Kriegel et al. (2009, 2011), Simon, Saur, Kriegel, et al. (2011), Saur et al. (2007), Simon et al. (2014), (10): Khurana et al. (2008), Simon et al. (2009), (11): Saur (2005), Simon, Saur, Neubauer, et al. (2011), (12): Khurana et al. (2008), Simon et al. (2012), Khurana et al. (2017) (13) Neubauer et al. (2006), Simon et al. (2010), Arridge et al. (2011), Bertucci et al. (2008) (14) Ness et al. (1986), Bridge et al. (1986), McNutt et al. (1987), (15) Neubauer (1990).

Planet	Satellite	Radius km (1)	Semi-Major R_P (2)	B_0 nT	v_0 km/s	n_p cm^{-3}	M_A	M_S	β	$\bar\alpha$ Eq. (5)	Comments	Ref.
Earth	Moon	1737.5	60.3	10	100	0.1	0.05	~1	<0.01	-	20 % of orbit in magnetosphere	(3)
Jupiter	Io	1821.3	6.0	1720	57	2500.	0.31	2.0	0.32	0.9-0.95	most powerful interaction	(4)
Jupiter	Europa	1565	9.6	370	76	200	0.47	0.9	0.32	0.8	induction in ocean	(5)
Jupiter	Ganymede	2634	15.3	64	139	5.	0.73	0.5	2.4	0.2	intrinsic dynamo field, induction	(6)
Jupiter	Callisto	2403	26.9	4	192	0.15	2.8	0.4	64	>0.99	enhanced ionospheric conductances	(7)
Saturn	Mimas	198.8	3.2	722	16	90	0.04	0.69	0.003	-	no in-situ observations	(8)
Saturn	Enceladus	252.3	4.1	325	26	70.5	0.13	1.32	0.01	>0.95	plumes, dusty plasma, hemisphere coup.	(9)
Saturn	Tethys	536.3	5.1	167	34	30	0.21	1.3	0.03	<0.03	wake effects	(10)
Saturn	Dione	562.5	6.5	75	40	13	0.37	0.89	0.2	~0.03	weak interaction	(11)
Saturn	Rhea	764.5	9.1	25	57	2	0.61	1.3	0.26	<0.15	wake effects dominate	(12)
Saturn	Titan	2575.5	21.0	~5	120	~0.1	~1	<1	>1	1	highly variable plasma environ.	(13)
Uranus	Ariel	578.9	7.5	80	9	0.15	0.002	0.02	0.01	-	no in-situ obs	(14)
Uranus	Umbriel	584.7	10.5	30	16	0.06	0.006	-	-	-	no in-situ obs	(14)
Uranus	Titania	788.9	17.2	7	30	0.021	0.03	-	-	-	no in-situ obs	(164)
Uranus	Oberon	761.4	23.0	3	42	0.016	0.09	-	-	-	no in-situ obs	(14)
Neptune	Triton	1352.6	14.4	10	39	-	0.1	-	-	-	no in-situ obs	(15)

the most powerful interaction. Io's interaction generates magnetic field perturbations of ~ 700 nT (Kivelson, Khurana, Walker, et al., 1996), it it radiates away in each Alfvén wings a Poynting flux of $\sim 1 \times 10^{12}$ W (Saur et al., 2013).

Since all moons are in many aspects similar to terrestrial type planets, there is a tremendous interest in using observations of their space environment to understand the interior structure of the moons. For Io, Khurana et al. (2011) argued that the magnetic field measurements taken during certain Galileo spacecraft flybys contain contributions which stem from induction in a 50 km thick magma ocean very close to the surface. The existence of such a surface near magma ocean (although plausible from considerations of Io's interior (Peale et al., 1979)) has been questioned based on Hubble Space Telescope observations of Io's auroral spot oscillation and MHD modeling with appropriate atmosphere models (Roth et al., 2017; Blöcker et al., 2018). Both, Europa and Ganymede exhibit induction signals from saline subsurface oceans (Khurana et al., 1998; Kivelson et al., 2000, 2002). In case of Ganymede, the induction signal based on observations during a single flyby are however non-unique due to Ganymede's internal dynamo magnetic field with its unknown quadrupole components. This non-uniqueness could be solved and the ocean could be confirmed with HST observations of reduced oscillation of Ganymede's auroral ovals due to induction in its saline subsurface ocean (Saur et al., 2015). Callisto was also argued to possess a subsurface ocean based on induction signals obtained during several Galileo spacecraft flybys (Khurana et al., 1998; Zimmer et al., 2000). Recently the uniqueness of this interpretation was questioned because of Callisto's highly conductive ionosphere which can significantly contribute to Callisto's magnetic field environment (Hartkorn & Saur, 2017).

Ganymede's interaction is unique because Ganymede's intrinsic dynamo magnetic field causes a mini-magnetosphere within Ganymede's larger magnetosphere. In contrast to the planetary magnetospheres for typical the solar wind conditions, it is a magnetosphere without a bow shock, but with Alfvén wings. Ganymede's magnetosphere is also particularly interesting for reconnection studies because of the much more steady setup compared to the interaction of the planetary magnetospheres with the solar wind since Jupiter's and Ganymede's magnetic moments are approximately anti-parallel (Neubauer, 1998; Ip & Kopp, 2002; Paty & Winglee, 2004; Jia et al., 2008; Poppe et al., 2018; Wang et al., 2018; Collinson et al., 2018; Tóth et al., 2016).

All Galilean moons possess dilute atmospheres (Strobel, 2005). The momentum-exchange of Jupiter's magnetospheric plasma with these atmospheres is therefore the key reason for the moon-magnetosphere interaction in case of Io, Europa and Callisto. Observations and modeling of magnetic field and plasma perturbations (Blöcker et al., 2016; Jia et al., 2018; Arnold et al., 2019) help to characterize the moons atmospheres (Hall et al., 1995) and to search for plumes originally detected with the Hubble Space Telescope (Roth et al., 2014). The mass loss from these atmospheres, in particular from Io and Europa, are primary plasma sources for Jupiter's magnetosphere. The most important mass loss is neutral sputtering with subsequent ionization within the magnetosphere. Total loss rates are about 10^3 kg s^{-1} of SO_2 for Io and 50 kg s^{-1} of O_2 for Europa (Bagenal & Delamere, 2011; V. Dols et al., 2008; Saur et al., 1998; Mauk et al., 2003; Saur, 2003; V. J. Dols et al., 2016).

The far-field interactions of the Galilean satellites are impressively visible in form of satellite footprints at wavelength ranging from the infrared to the ultraviolet (Figure 1 and, e.g., Connerney et al. (1993); Prangé et al. (1996); Clarke et al. (1996); Ingersoll et al. (1998); Clarke et al. (2002); Bhattacharyya et al. (2018)). The footprints show a complex structure consisting of a main spot, a leading spot, i.e., in front of the main spot, at footprint tail and sometimes multiple spots (Bonfond et al., 2008; Grodent et al., 2009). The main spot is caused by the primary Alfvén wing and its associated electron particle acceleration. The leading spots result from trans-hemispheric electron beams as part of the bi-directional electron acceleration within the main wing (Bonfond et al., 2008).

The tails and the multiple spots within the tails are generated by the reflected Alfvén waves at the torus boundaries and other density gradients along the magnetospheric field lines (Neubauer, 1980; Jacobsen et al., 2007). Depending on the strength of the interaction at the moon (i.e., when the moon is in the magnetospheric plasma sheet or outside), the reflection of the wave can be highly non-linear where incident and reflection angle are different. The non-linear interaction can smear out multiple spots in the tail (Jacobsen et al., 2007). Very recently, observation with unprecedented spatial resolution in the infrared by the JUNO spacecraft revealed detailed substructures of the multiple spots (Mura et al., 2018). These are in appearance reminiscent of von Karman streets known from hydrodynamics, but not in the underlying physics.

The physics of particle acceleration in the main wings and their tails is poorly constrained, but at the time of writing this chapter for the first time being probed with in-situ measurements by the Juno spacecraft. Based on Juno measurements, Szalay et al. (2018) found broadband bidirectional electron beams in the high latitude wake region of Io consistent with stochastic acceleration of reflected Alfvén waves (Hess et al., 2010; Bonfond et al., 2017).

5.3 Saturn: Titan and icy satellites

The moons of Saturn, which are permanently located within its magnetosphere are Mimas, Enceladus, Tethys, Dione, Rhea. Titan can be located outside the magnetosphere under exceptional solar wind conditions. These bodies are all icy moons with Titan and Enceladus being arguably the scientifically most exciting objects among Saturn's moons.

Mimas, Tethys, Dione and Rhea are icy moons with thin exospheres. These exospheres generate only a minor perturbation to the magnetospheric plasma flow and magnetic field. However, these moons act as absorbers of the upstream plasma and thus generate empty wakes which are increasingly filled with plasma further downstream driven by slow mode waves and accompanied by rarefaction waves away from the wake. The associated movement of plasma and the resultant magnetic field perturbation partially propagate away as Alfvén waves contributing to the moons Alfvén wings (Simon et al., 2009, 2012; Khurana et al., 2017).

Enceladus provided a huge surprise to the Cassini Mission. Within four rifts in its icy crust nicknamed 'tiger stripes', water vapor plumes emerge. These plumes provide obstacles to the magnetospheric flow and generate magnetic field perturbations, which were observed by the spacecraft and successively led to the detection of the plumes with the other Cassini instruments (Dougherty et al., 2006; Porco et al., 2006). These plumes are the major plasma source of Saturn's magnetosphere (Fleshman et al., 2010; Smith et al., 2010). The plumes provide several new interesting components of moon-magnetosphere interaction. Since the plumes are located below the south pole, the northern Alfvén wing starts already in the southern hemisphere. The northern wing is then partially blocked by the absorbing insulating icy body, which leads to hemisphere coupling currents and associated magnetic field discontinuities on field lines tangent to the body (Saur et al., 2007; Simon et al., 2014). The plumes' gas contains a significant amount of dust in form of mostly micrometer sized ice particles, which are negatively charged, and thus render a complex dusty plasma around Enceladus (Hill et al., 2012). The negatively charged dust reverses the sign of the Hall conductivity within the plume (Simon, Saur, Kriegel, et al., 2011; Kriegel et al., 2011). Enceladus' plasma interaction experiences time-variability due to the variability of the outgassing from the plumes caused by tidal stresses along its eccentric orbit around Saturn (Saur et al., 2008; Hedman et al., 2013).

Titan is also an exceptional moon in many aspects. It possesses a nitrogen rich atmosphere with an atmospheric surface pressure of 1.5 bar. It is thus the only moon where the surrounding plasma does not reach the surface of the moon. It possesses an ionosphere and is subject to a highly variable plasma and field field environment because Ti-

tan orbits Saturn close to its magnetopause (Rymer et al., 2009; Simon et al., 2010). Due to the large plasma beta mostly as a results of the low magnetic field strength at the orbit of Titan, the plasma is strongly draped around Titan's atmosphere and ionosphere (Ma et al., 2006; Modolo & Chanteur, 2008). Because of the very low plasma velocities in Titan's ionosphere and the partly frozen-in magnetic fields, time-variable external magnetic fields from previous times (up to several hours) are still observable in its ionosphere. These fields are referred to as fossil fields (Neubauer et al., 2006; Bertucci et al., 2008). For a comprehensive discussion about Titan's interaction we refer the reader to a separate chapter by C. Bertucci.

5.4 Uranus: Icy moons

Uranus harbors four moons with diameters larger than 1000 km within its magnetosphere. They are Ariel, Umbriel, Titania and Oberon. The only spacecraft to perform in-situ observation of Uranus' magnetosphere was the Voyager 2 spacecraft, but it did not pass the moons at close enough distances to detect signatures of moon-magnetosphere interaction. Voyager 2 found that Uranus' magnetosphere, compared to those of Jupiter and Saturn, is only sparsely populated with plasma. The expected plasma and magnetic field values near the moons are displayed in table 1. No atmospheres or exospheres around the moons are observed. Thus the plasma interactions generated by the moons are expected to be very weak.

The large icy moons might harbor subsurface water oceans (Hussmann et al., 2006). The magnetic moment of Uranus is tilted by approximately 60° with respect to its spin axis (Ness et al., 1986), which will result in large amplitude time-periodic magnetic fields at the locations of the moons. In case of electrically conductive oceans, large dipole magnetic fields will be induced and be measurable outside of the moons (Saur et al., 2010). These time-variable induced dipole fields will also generate a weak far-field interaction in form of Alfvén wings.

5.5 Neptune: Triton

In the Neptune system, Triton is the only moon with diameter larger than 1000 km. Triton is a moon with a thin atmosphere and small scale plumes out of methane. Thus the interaction of the magnetospheric plasma with the atmosphere of Triton will generate an active, i.e., $\bar{\alpha} > 0$ plasma interaction, which however has not been observationally confirmed. Voyager 2 was so far the only spacecraft to visit Neptune but without a sufficiently close encounter with Triton to detect its moon-magnetosphere interaction. Neptune's magnetic moment is inclined by 47° with respect to its spin axis (Ness et al., 1989). Triton in addition possesses an inclination of 156.8°. Therefore an observer in the rest frame of Titan sees a highly time-variable magnetic field at both the synodic rotation period of Neptune (14.46 h) and the orbital period of Triton (5.88 d) (Saur et al., 2010). Any saline subsurface water ocean as discussed in the literature (Hussmann et al., 2006), will generate easily observable induction signals at close flybys.

5.6 Extrasolar planets: Star-planet interaction

The equivalent of moons in planetary magnetospheres in other stellar systems are close-in extra solar planets interacting with their stellar astrospheres. If the close-in extra solar planets are within the Alfvén radius of the associated stellar wind (defined by the location with $M_A = 1$), then the exoplanets are subject to sub-Alfvénic interaction. Within that radius the interaction of the stellar wind with the exoplanet can generate Alfvén wings which can reach the central star. This counterpart to moon-magnetosphere interaction is called electromagnetic 'star-planet interaction'. Observational evidence comes, e.g., from correlation of stellar Ca II emission with the orbital period of a close-in exoplanet (Shkolnik et al., 2008). Theoretical studies on star-planet interaction have been

performed numerically and analytically by Cuntz et al. (2000); Preusse et al. (2005); Zarka (2007); Lanza (2008); Saur et al. (2013); Strugarek et al. (2015); Turnpenney et al. (2018).

6 Outstanding questions

Finally we discuss several open questions in the field of moon-magnetosphere interaction:

The far-field interaction introduced in Section 4.2 is observationally as well as theoretically the least understood part of moon-magnetosphere interaction. It is in many aspects unclear how the Alfvén waves evolve while traveling towards the planets. In particular, the reflection and filamentation processes which are expected to take place are of key interest (Chust et al., 2005; Hess et al., 2010; Hess & Delamere, 2013). Also the acceleration processes where the Alfvén wave energy is converted into accelerated electrons and ions, which lead to the satellite footprint emission in the planets' atmospheres has been barely investigated. Here relativistic effects also play a role in parts of the magnetospheres with v_A from (1) assuming values larger then the speed of light and with electron energies larger than a few hundred keV. Further studies will hopefully also shed light into understanding the enigmatic tail features of the Io footprints recently observed by the JUNO spacecraft (Mura et al., 2018). The coupling of the Alfvén wings to the planets' ionospheres is also a very poorly studied subject. Models for the coupling between the wings and the ionospheres will require the inclusion of the steep density gradients and the consideration of anisotropic ionospheric conductivities.

Even though the local interaction introduced in Section 4.1 is much better understood than the far-field interaction, the non-linear interaction of the various processes, such as plasma interaction in the atmospheres, induction in the interiors and ionospheres, and atmosphere-plasma feedback are only poorly investigated. The later points address how the plasma interaction contributes to the generation, loss and reshaping of the dilute moon-atmospheres.

Ultimately, it will be necessary to combine the near-field, the far-field and the coupling to the planets' ionosphere for obtaining a 'global' understanding of moon-magnetosphere interaction. This includes an understanding of the linear momentum, angular momentum and energy fluxes between the moons and their planets.

The moon-magnetosphere interaction of the moons of Uranus and Neptune are observationally only weakly constrained and therefore new space missions to these two planets are highly desirable (Arridge et al., 2014; Christophe et al., 2012).

A better cross-comparison of moon-magnetosphere interaction and star-planet interaction in extrasolar systems would also be highly desirable as the similarities and differences taking place in these systems are not sufficiently investigated. Efforts in this area would additional help to bridge the space physics community of the solar system with the astronomical community and will contribute to unify planetary sciences across their borders.

References

Acton, C. H. (1996, January). Ancillary data services of NASA's Navigation and

Ancillary Information Facility. *Plantary and Space Science*, *44*, 65-70. doi: 10
.1016/0032-0633(95)00107-7

Acuña, M. H., Neubauer, F. M., & Ness, N. F. (1981). Standing Alfvén wave current
system at Io : Voyager-1 observations. *J. Geophys. Res.*, *86*, 8513-8521.

Arnold, H., Liuzzo, L., & Simon, S. (2019). Magnetic signatures of a plume at eu-
ropa during the galileo e26 flyby. *Geophysical Research Letters*, *46*(3), 1149-
1157. doi: 10.1029/2018GL081544

Arridge, C. S., Achilleos, N., Agarwal, J., Agnor, C. B., Ambrosi, R., André, N., . . .
Zarka, P. (2014, December). The science case for an orbital mission to Uranus:
Exploring the origins and evolution of ice giant planets. *Planet. Space Sci.*,
104, 122-140. doi: 10.1016/j.pss.2014.08.009

Arridge, C. S., André, N., Bertucci, C. L., Garnier, P., Jackman, C. M., Németh,
Z., . . . Crary, F. J. (2011, December). Upstream of Saturn and Titan.
Space Sci. Rev., *162*, 25-83. doi: 10.1007/s11214-011-9849-x

Backes, H., et al. (2005). Titan's magnetic field signature during the first Cassini en-
counter. *Science*, *308*, 992-995.

Bagenal, F., & Delamere, P. A. (2011, May). Flow of mass and energy in the mag-
netospheres of Jupiter and Saturn. *Journal of Geophysical Research (Space
Physics)*, *116*, A05209. doi: 10.1029/2010JA016294

Baumjohann, W., & Treumann, R. A. (2012). *Basic Space Plasma Physics.* London:
Imperial College Press.

Bertucci, C., Achilleos, N., Dougherty, M. K., Modolo, R., Coates, A. J., Szego, K.,
. . . Young, D. T. (2008, September). The Magnetic Memory of Titan's Ionized
Atmosphere. *Science*, *321*, 1475. doi: 10.1126/science.1159780

Bhattacharyya, D., Clarke, J. T., Montgomery, J., Bonfond, B., Gérard, J.-C., &
Grodent, D. (2018, January). Evidence for Auroral Emissions From Cal-
listo's Footprint in HST UV Images. *Journal of Geophysical Research (Space
Physics)*, *123*, 364-373. doi: 10.1002/2017JA024791

Bigg, E. K. (1964). Influence of the satellite Io on Jupiter's decametric emission. *Na-
ture*, *203*, 1008-1010.

Blöcker, A., Saur, J., & Roth, L. (2016, October). Europa's plasma interaction
with an inhomogeneous atmosphere: Development of Alfvén winglets within
the Alfvén wings. *Journal of Geophysical Research (Space Physics)*, *121*,
9794-9828. doi: 10.1002/2016JA022479

Blöcker, A., Saur, J., Roth, L., & Strobel, D. (2018). MHD Modeling of the Plasma
Interaction with Io's Asymmetric Atmosphere. *Journal of Geophysical Re-
search (Space Physics)*, In revision.

Bonfond, B., Grodent, D., Gérard, J., Radioti, A., Saur, J., & Jacobsen, S. (2008,
March). UV Io footprint leading spot: A key feature for understanding the UV
Io footprint multiplicity? *grl*, *35*, L05107. doi: 10.1029/2007GL032418

Bonfond, B., Saur, J., Grodent, D., Badman, S. V., Bisikalo, D., Shematovich, V.,
. . . Radioti, A. (2017, August). The tails of the satellite auroral footprints at
Jupiter. *Journal of Geophysical Research (Space Physics)*, *122*, 7985-7996. doi:
10.1002/2017JA024370

Bridge, H. S., Belcher, J. W., Coppi, B., Lazarus, A. J., McNutt, R. L., Olbert, S.,
. . . Eviatar, A. (1986, July). Plasma observations near Uranus - Initial results
from Voyager 2. *Science*, *233*, 89-93. doi: 10.1126/science.233.4759.89

Bridge, H. S., et al. (1979, June). Plasma observations near Jupiter: Initial results
from Voyager 1. *Science*, *204*(4396), 987-991.

Broadfoot, A. L., et al. (1979). Extreme ultraviolet observations from Voyager 1 en-
counter with Jupiter. *Science*, *204*, 979-982.

Christophe, B., Spilker, L. J., Anderson, J. D., André, N., Asmar, S. W., Aurnou,
J., . . . Wolf, P. (2012, October). OSS (Outer Solar System): a fundamen-
tal and planetary physics mission to Neptune, Triton and the Kuiper Belt.
Experimental Astronomy, *34*, 203-242. doi: 10.1007/s10686-012-9309-y

Chust, T., et al. (2005). Are Io's Alfvén wings filamented? Galileo observations. *Plantary and Space Science*, *53*, 395-412.

Clarke, J. T., Ajello, J., Ballester, G. E., Jaffel, L. B., Connerney, J. E. P., Gérard, J.-C., ... Waite, J. H. (2002, February). Ultaviolet emissions from the magnetic footprints of Io, Ganymede and Europa on Jupiter. *Nature*, *415*, 997-1000.

Clarke, J. T., et al. (1996, October). Far-ultraviolet imaging of Jupiter's aurora and the Io "Footprint". *Science*, *274*(5286), 404-409.

Collinson, G., Paterson, W. R., Bard, C., Dorelli, J., Glocer, A., Sarantos, M., & Wilson, R. (2018, April). New Results From Galileo's First Flyby of Ganymede: Reconnection-Driven Flows at the Low-Latitude Magnetopause Boundary, Crossing the Cusp, and Icy Ionospheric Escape. *Geophys. Res. Lett.*, *45*, 3382-3392. doi: 10.1002/2017GL075487

Connerney, J. E. P., Baron, R., Satoh, T., & Owen, T. (1993, November). Images of excited H_3^+ at the foot of the Io flux tube in Jupiter's atmosphere. *Science*, *262*(5316), 1035-1038.

Cowling, T. G. (1932, November). Magnetism, Solar : The electrical conductivity of an ionised gas in the presence of a magnetic field. *mnras*, *93*, 90. doi: 10.1093/mnras/93.1.90

Crary, F. J. (1997, January). On the generation of an electron beam by Io. *J. Geophys. Res.*, *102*(A1), 37-49.

Cuntz, M., Saar, S. H., & Musielak, Z. E. (2000, April). On Stellar Activity Enhancement Due to Interactions with Extrasolar Giant Planets. *Astrophys. J. Lett.*, *533*, L151-L154. doi: 10.1086/312609

Dols, V., Delamere, P. A., & Bagenal, F. (2008, September). A multispecies chemistry model of Io's local interaction with the Plasma Torus. *Journal of Geophysical Research (Space Physics)*, *113*, A09208. doi: 10.1029/2007JA012805

Dols, V. J., Bagenal, F., Cassidy, T. A., Crary, F. J., & Delamere, P. A. (2016, January). Europa's atmospheric neutral escape: Importance of symmetrical O_2 charge exchange. *Icarus*, *264*, 387-397. doi: 10.1016/j.icarus.2015.09.026

Dougherty, M. K., Khurana, K. K., Neubauer, F. M., Russell, C. T., Saur, J., Leisner, J. S., & Burton, M. (2006). Identification of a dynamic atmosphere at Enceladus with the Cassini Magnetometer. *Science*, *311*, 1406.

Duling, S., Saur, J., & Wicht, J. (2014, June). Consistent boundary conditions at nonconducting surfaces of planetary bodies: Applications in a new Ganymede MHD model. *Journal of Geophysical Research (Space Physics)*, *119*, 4412-4440. doi: 10.1002/2013JA019554

Elsässer, W. (1950). The hydromagnetic equations. *Phys. Rev.*, *79*, 183. doi: 10.1103/PhysRev.79.183

Eviatar, A., Strobel, D. F., Wolfven, B. C., Feldman, P., McGrath, M. A., & Williams, D. J. (2001). Excitation of the Ganymede ultraviolet aurora. *Astrophys. J.*, *555*, 1013-1019.

Fleshman, B. L., Delamere, P. A., & Bagenal, F. (2010, February). Modeling the Enceladus plume-plasma interaction. *Geophys. Res. Lett.*, *37*, L03202. doi: 10.1029/2009GL041613

Goertz, C. K. (1980). Io's interaction with the plasma torus. *J. Geophys. Res.*, *85*(A6), 2949-2956.

Goldreich, P., & Lynden-Bell, D. (1969). Io, a Jovian unipolar inductor. *Astrophys. J.*, *156*, 59-78.

Grodent, D., Bonfond, B., Radioti, A., Gérard, J., Jia, X., Nichols, J. D., & Clarke, J. T. (2009, July). Auroral footprint of Ganymede. *Journal of Geophysical Research (Space Physics)*, *114*, A07212. doi: 10.1029/2009JA014289

Halekas, J. S., Poppe, A. R., Farrell, W. M., Delory, G. T., Angelopoulos, V., McFadden, J. P., ... Ergun, R. E. (2012, May). Lunar precursor effects in the solar wind and terrestrial magnetosphere. *Journal of Geophysical Research*

(Space Physics), *117*, A05101. doi: 10.1029/2011JA017289

Hall, D. T., Strobel, D. F., Feldman, P. D., McGrath, M. A., & Weaver, H. A. (1995, February). Detection of an oxygen atmosphere on Jupiter's moon Europa. *Nature*, *373*(6516), 677-679.

Harnett, E. M., Cash, M., & Winglee, R. M. (2013, May). Substorm and storm time ionospheric particle flux at the Moon while in the terrestrial magnetosphere. *icarus*, *224*, 218-227. doi: 10.1016/j.icarus.2013.02.022

Hartkorn, O., & Saur, J. (2017, November). Induction signals from Callisto's ionosphere and their implications on a possible subsurface ocean. *Journal of Geophysical Research (Space Physics)*, *122*(A11), 11. doi: 10.1002/2017JA024269

Hartkorn, O., Saur, J., & Strobel, D. F. (2017, January). Structure and density of Callistos atmosphere from a fluid-kinetic model of its ionosphere: Comparison with Hubble Space Telescope and Galileo observations. *Journal of Geophysical Research (Planets)*, *282*, 237-259. doi: 10.1016/j.icarus.2016.09.020

Hedman, M. M., Gosmeyer, C. M., Nicholson, P. D., Sotin, C., Brown, R. H., Clark, R. N., . . . Showalter, M. R. (2013, August). An observed correlation between plume activity and tidal stresses on Enceladus. *Nature*, *500*, 182-184. doi: 10.1038/nature12371

Hess, S., & Delamere, P. A. (2013). Satellite-induced electron acceleration and related auroras. In *Auroral phenomenology and magnetospheric processes: Earth and other planets* (p. 295-304). American Geophysical Union (AGU). doi: 10.1029/2011GM001175

Hess, S. L. G., Delamere, P., Dols, V., Bonfond, B., & Swift, D. (2010, June). Power transmission and particle acceleration along the Io flux tube. *Journal of Geophysical Research (Space Physics)*, *115*, A06205. doi: 10.1029/2009JA014928

Hess, S. L. G., Delamere, P. A., Dols, V., & Ray, L. C. (2011). Comparative study of the power transferred from satellite-magnetosphere interactions to auroral emissions. *Journal of Geophysical Research (Space Physics)*, *116*, A01202. doi: 10.1029/2010JA015807

Hill, T. W., Thomsen, M. F., Tokar, R. L., Coates, A. J., Lewis, G. R., Young, D. T., . . . Horányi, M. (2012, May). Charged nanograins in the Enceladus plume. *Journal of Geophysical Research (Space Physics)*, *117*, A05209. doi: 10.1029/2011JA017218

Hussmann, H., Sohl, F., & Spohn, T. (2006). Subsurface oceans and deep interiors of medium-sized outer planet satellites and large trans-neptunian objects. *Icarus*, *185*, 258-273.

Ingersoll, A. P., Vasavada, A. R., Little, B., Anger, C. D., Bolton, S. J., Alexander, C., . . . Galileo SSI Team (1998, September). Imaging Jupiter's Aurora at Visible Wavelengths. *Icarus*, *135*, 251-264. doi: 10.1006/icar.1998.5971

Ip, W., & Kopp, A. (2002). Resistive MHD simulations of Ganymede's magnetosphere: 2. Birkeland currents and particle energetics. *J. Geophys. Res.*, *107*, CiteID 1491.

Jacobsen, S., Neubauer, F. M., Saur, J., & Schilling, N. (2007). Io's nonlinear MHD-wave field in the heterogeneous Jovian magnetosphere. *Geophys. Res. Lett.*, *34*(doi:10.1029/2006GL029187), L10202.

Jacobsen, S., Saur, J., Neubauer, F. M., Bonfond, B., Gérard, J., & Grodent, D. (2010, April). Location and spatial shape of electron beams in Io's wake. *J. Geophys. Res.*, *115*, A4205. doi: 10.1029/2009JA014753

Jia, X., Kivelson, M. G., Khurana, K. K., & Kurth, W. S. (2018, June). Evidence of a plume on Europa from Galileo magnetic and plasma wave signatures. *Nature Astronomy*, *2*, 459-464. doi: 10.1038/s41550-018-0450-z

Jia, X., Walker, R., Kivelson, M., Khurana, K., & Linker, J. (2008). Three-dimensional MHD simulations of Ganymede's magnetosphere. *J. Geophys. Res.*, *113*, A06212.

Khurana, K. K., Fatemi, S., Lindkvist, J., Roussos, E., Krupp, N., Holmström, M.,

... Dougherty, M. K. (2017, February). The role of plasma slowdown in the generation of Rhea's Alfvén wings. *Journal of Geophysical Research (Space Physics)*, *122*, 1778-1788. doi: 10.1002/2016JA023595

Khurana, K. K., Jia, X., Kivelson, M. G., Nimmo, F., Schubert, G., & Russell, C. T. (2011, June). Evidence of a Global Magma Ocean in Io's Interior. *Science*, *332*, 1186. doi: 10.1126/science.1201425

Khurana, K. K., Kivelson, M. G., & Russell, C. T. (2002). Searching for liquid water in Europa by using surface observations. *Astrobiol. J.*, *2*, 93-103.

Khurana, K. K., Kivelson, M. G., Stevenson, D. J., Schubert, G., Russell, C. T., Walker, R. J., & Polanskey, C. (1998). Induced magnetic fields as evidence for subsurface oceans in Europa and Callisto. *Nature*, *395*, 777-780.

Khurana, K. K., Russell, C. T., & Dougherty, M. K. (2008, February). Magnetic portraits of Tethys and Rhea. *Icarus*, *193*, 465-474. doi: 10.1016/j.icarus.2007 .08.005

Kivelson, M. G., Bagenal, F., Neubauer, F. M., Kurth, W., Paranicas, C., & Saur, J. (2004). Magnetospheric interactions with satellites. In F. Bagenal (Ed.), *Jupiter* (p. 513-536). University of Colorado: Cambridge Univ. Press.

Kivelson, M. G., Khurana, K. K., Russell, C. T., Volwerk, M., Walker, J., & Zimmer, C. (2000). Galileo magnetometer measurements: A stronger case for a subsurface ocean at Europa. *Science*, *289*(5483), 1340-1343.

Kivelson, M. G., Khurana, K. K., Russell, C. T., Walker, R. J., Warnecke, J., Coroniti, F. V., ... Schubert, G. (1996). Discovery of Ganymede's magnetic field by the Galileo spacecraft. *Nature*, *384*, 537-541.

Kivelson, M. G., Khurana, K. K., & Volwerk, M. (2002). The permanent and inductive magnetic moments of Ganymede. *Icarus*, *157*, 507-522.

Kivelson, M. G., Khurana, K. K., Walker, R. J., Russell, C. T., Linker, J. A., Southwood, D. J., & Polanskey, C. (1996). A magnetic signature at Io: Initial report from the Galileo magnetometer. *Science*, *273*, 337-340.

Kliore, A. J., Fjeldbo, G., Seidel, B. L., Sweetnam, D. N., Sesplaukis, T. T., Woiceshyn, P. M., & Rasool, S. I. (1975). The atmosphere of Io from Pioneer 10 radio occultation measurement. *Icarus*, *24*, 407-410.

Kriegel, H., Simon, S., Motschmann, U., Saur, J., Neubauer, F. M., Persoon, A. M., ... Gurnett, D. A. (2011, October). Influence of negatively charged plume grains on the structure of Enceladus' Alfvén wings: Hybrid simulations versus Cassini Magnetometer data. *Journal of Geophysical Research (Space Physics)*, *116*, 10223. doi: 10.1029/2011JA016842

Kriegel, H., Simon, S., Müller, J., Motschmann, U., Saur, J., Glassmeier, K., & Dougherty, M. K. (2009, December). The plasma interaction of Enceladus: 3D hybrid simulations and comparison with Cassini MAG data. *Planetary and Space Science*, *57*, 2113-2122. doi: 10.1016/j.pss.2009.09.025

Lagg, A., Krupp, N., Woch, J., & Williams, D. J. (2003, June). In-situ observations of a neutral gas torus at Europa. *Geophys. Res. Lett.*, *30*(11), 4039-4042.

Lanza, A. F. (2008, September). Hot Jupiters and stellar magnetic activity. *Astron. Astrophys.*, *487*, 1163-1170. doi: 10.1051/0004-6361:200809753

Liuzzo, L., Feyerabend, M., Simon, S., & Motschmann, U. (2015, November). The impact of Callisto's atmosphere on its plasma interaction with the Jovian magnetosphere. *Journal of Geophysical Research (Space Physics)*, *120*, 9401-9427. doi: 10.1002/2015JA021792

Louis, C. K., Lamy, L., Zarka, P., Cecconi, B., & Hess, S. L. G. (2017, September). Detection of Jupiter decametric emissions controlled by Europa and Ganymede with Voyager/PRA and Cassini/RPWS. *Journal of Geophysical Research (Space Physics)*, *122*, 9228-9247. doi: 10.1002/2016JA023779

Ma, Y., Nagy, A. F., Cravens, T. E., Sokolov, I. V., Hansen, K. C., Wahlund, J.-E., ... Dougherty, M. K. (2006, May). Comparisons between MHD model calculations and observations of Cassini flybys of Titan. *Journal of Geophysical*

Research (Space Physics), *111*, A05207. doi: 10.1029/2005JA011481

Mauk, B., Mitchell, D., Krimigis, S., Roelof, E., & Paranicas, C. (2003). Energetic neutral atoms from a trans-Europa gas torus at Jupiter. *Nature*, *412*(6926), 920-922.

Mauk, B. H., Mitchell, D. G., McEntire, R. W., Paranicas, C. P., Roelof, E. C., Williams, D. J., . . . Lagg, A. (2004, September). Energetic ion characteristics and neutral gas interactions in Jupiter's magnetosphere. *Journal of Geophysical Research (Space Physics)*, *109*, A09S12. doi: 10.1029/2003JA010270

McNutt, R. L., Selesnick, R. S., & Richardson, J. D. (1987, May). Low-energy plasma observations in the magnetosphere of Uranus. *J. Geophys. Res.*, *92*, 4399-4410. doi: 10.1029/JA092iA05p04399

Modolo, R., & Chanteur, G. M. (2008, January). A global hybrid model for Titan's interaction with the Kronian plasma: Application to the Cassini Ta flyby. *Journal of Geophysical Research (Space Physics)*, *113*, A01317. doi: 10.1029/2007JA012453

Mura, A., Adriani, A., Connerney, J. E. P., Bolton, S., Altieri, F., Bagenal, F., . . . Turrini, D. (2018, August). Juno observations of spot structures and a split tail in Io-induced aurorae on Jupiter. *Science*, *361*, 774-777. doi: 10.1126/science.aat1450

Ness, N. F., Acuña, M. H., Behannon, K. W., Burlaga, L. F., Connerney, J., Lepping, R. P., & Neubauer, F. M. (1986). Magnetic fields at Uranus. *Science*, *233*, 85-89.

Ness, N. F., Acuña, M. H., Burlaga, L. F., Connerney, J., Lepping, R. P., & Neubauer, F. M. (1989). Magnetic fields at Neptune. *Science*, *246*, 1473-1478.

Neubauer, F. M. (1980, March). Nonlinear standing Alfvén wave current system at Io: Theory. *J. Geophys. Res.*, *85*(A3), 1171-1178.

Neubauer, F. M. (1990). Satellite plasma interaction. *Adv. Space Res.*, *10*(1), 25-38.

Neubauer, F. M. (1998, September). The sub-Alfvénic interaction of the Galilean satellites with the Jovian magnetosphere. *J. Geophys. Res.*, *103*(E9), 19843-19866.

Neubauer, F. M., Backes, H., Dougherty, M. K., Wennmacher, A., Russell, C. T., Coates, A., . . . Saur, J. (2006, October). Titan's near magnetotail from magnetic field and electron plasma observations and modeling: Cassini flybys TA, TB, and T3. *Journal of Geophysical Research (Space Physics)*, *111*, A10220. doi: 10.1029/2006JA011676

Paty, C., & Winglee, R. (2004). Multi-fluid simulations of Ganymede's magnetosphere. *Geophys. Res. Lett.*, *31*, L24806.

Peale, S. J., Cassen, P., & Reynolds, R. T. (1979, March). Melting of Io by tidal dissipation. *Science*, *203*, 892-894.

Poppe, A. R., Fatemi, S., & Khurana, K. K. (2018, June). Thermal and Energetic Ion Dynamics in Ganymede's Magnetosphere. *Journal of Geophysical Research (Space Physics)*, *123*, 4614-4637. doi: 10.1029/2018JA025312

Porco, C., et al. (2006). Cassini observes the active south pole of Enceladus. *Science*, *311*, 1393-1401.

Prangé, R., Rego, D., Southwood, D., Zarka, P., Miller, S., & Ip, W.-H. (1996, January). Rapid energy dissipation and variability of the Io-Jupiter electrodynamic circuit. *Nature*, *379*(6563), 323-325.

Preusse, S., Kopp, A., Büchner, J., & Motschmann, U. (2005, May). Stellar wind regimes of close-in extrasolar planets. *Astron. Astrophys.*, *434*, 1191-1200. doi: 10.1051/0004-6361:20041680

Pryor, W. R., Rymer, A. M., Mitchell, D. G., Hill, T. W., Young, D. T., Saur, J., . . . Zhou, X. (2011, April). The auroral footprint of Enceladus on Saturn. *Nature*, *472*, 331-333. doi: 10.1038/nature09928

Rees, M. H. (1989). *Physics and Chemistry of the Upper Atmosphere*. New York: Cambridge Univ. Press.

Roth, L., Saur, J., Retherford, K. D., Blöcker, A., Strobel, D. F., & Feldman, P. D. (2017, February). Constraints on Io's interior from auroral spot oscillations. *Journal of Geophysical Research (Space Physics)*, *122*, 1903-1927. doi: 10.1002/2016JA023701

Roth, L., Saur, J., Retherford, K. D., Strobel, D. F., Feldman, P. D., McGrath, M. A., & Nimmo, F. (2014, January). Transient Water Vapor at Europa's South Pole. *Science*, *343*, 171-174. doi: 10.1126/science.1247051

Rubin, M., Jia, X., Altwegg, K., Combi, M. R., Daldorff, L. K. S., Gombosi, T. I., ... Wurz, P. (2015, May). Self-consistent multifluid MHD simulations of Europa's exospheric interaction with Jupiter's magnetosphere. *Journal of Geophysical Research (Space Physics)*, *120*, 3503-3524. doi: 10.1002/2015JA021149

Rymer, A. M., Smith, H. T., Wellbrock, A., Coates, A. J., & Young, D. T. (2009, August). Discrete classification and electron energy spectra of Titan's varied magnetospheric environment. *Geophys. Res. Lett.*, *36*, L15109. doi: 10.1029/2009GL039427

Saur, J. (2004). A model for Io's local electric field for a combined Alfvénic and unipolar inductor far-field coupling. *J. Geophys. Res.*, *109*, A01210.

Saur, J., Duling, S., Roth, L., Jia, X., Strobel, D. F., Feldman, P. D., ... Hartkorn, O. (2015, March). The search for a subsurface ocean in Ganymede with Hubble Space Telescope observations of its auroral ovals. *Journal of Geophysical Research (Space Physics)*, *120*, 1715-1737. doi: 10.1002/2014JA020778

Saur, J., Grambusch, T., Duling, S., Neubauer, F. M., & Simon, S. (2013, April). Magnetic energy fluxes in sub-Alfvénic planet star and moon planet interactions. *Astron. Astrophys.*, *552*, A119. doi: 10.1051/0004-6361/201118179

Saur, J., Janser, S., Schreiner, A., Clark, G., Mauk, B. H., Kollmann, P., ... Kotsiaros, S. (2018, November). Wave-Particle Interaction of Alfvén Waves in Jupiter's Magnetosphere: Auroral and Magnetospheric Particle Acceleration. *Journal of Geophysical Research (Space Physics)*, *123*, 9560-9573. doi: 10.1029/2018JA025948

Saur, J., Neubauer, F. M., & Glassmeier, K.-H. (2010). Induced magnetic fields in solar system bodies. *Space Sci. Rev.*, *152*, 391-421. doi: 10.1007/s11214-009-9581-y

Saur, J., Neubauer, F. M., & Schilling, N. (2007). Hemisphere coupling in Enceladus' asymmetric plasma interaction . *J. Geophys. Res.*, *112*, A11209, doi:10.1029/2007JA012479.

Saur, J., Neubauer, F. M., Strobel, D. F., & Summers, M. E. (1999, November). Three-dimensional plasma simulation of Io's interaction with the Io plasma torus: Asymmetric plasma flow. *J. Geophys. Res.*, *104*(A11), 25105-25126.

Saur, J., Schilling, N., Neubauer, F. M., et al. (2008). Evidence for temporal variability of enceladus' gas jets: Modeling of cassini observations. *Geophys. Res. Lett.*, *35*, L20105.

Saur, J., & Strobel, D. (2005). Atmospheres and plasma interactions at Saturn's largest inner icy satellites. *Astrophys. J. Lett.*, *620*, L115-L118.

Saur, J., Strobel, D. F., & Neubauer, F. M. (1998, August). Interaction of the Jovian magnetosphere with Europa: Constraints on the neutral atmosphere. *J. Geophys. Res.*, *103*(E9), 19947-19962.

Schilling, N., Neubauer, F. M., & Saur, J. (2007, June). Time-varying interaction of Europa with the jovian magnetosphere: Constraints on the conductivity of Europa's subsurface ocean. *Icarus*, *192*, 41-55.

Schilling, N., Neubauer, F. M., & Saur, J. (2008). Influence of the internally induced magnetic field on the plasma interaction of Europa. *J. Geophys. Res.*, *113*, A03203.

Seufert, M., Saur, J., & Neubauer, F. M. (2011, August). Multi-frequency electromagnetic sounding of the Galilean moons. *Icarus*, *214*, 477-494. doi: 10.1016/j.icarus.2011.03.017

Shkolnik, E., Bohlender, D. A., Walker, G. A. H., & Collier Cameron, A. (2008, March). The On/Off Nature of Star-Planet Interactions. *Astrophys. J.*, *676*, 628-638. doi: 10.1086/527351

Simon, S., Kriegel, H., Saur, J., Wennmacher, A., Neubauer, F. M., Roussos, E., . . . Dougherty, M. K. (2012, July). Analysis of Cassini magnetic field observations over the poles of Rhea. *Journal of Geophysical Research (Space Physics)*, *117*, 7211. doi: 10.1029/2012JA017747

Simon, S., Saur, J., Kriegel, H., Neubauer, F. M., Motschmann, U., & Dougherty, M. K. (2011, April). Influence of negatively charged plume grains and hemisphere coupling currents on the structure of Enceladus' Alfvén wings: Analytical modeling of Cassini magnetometer observations. *J. Geophys. Res.*, *116*, A04221. doi: 10.1029/2010JA016338

Simon, S., Saur, J., Neubauer, F. M., Motschmann, U., & Dougherty, M. K. (2009, February). Plasma wake of Tethys: Hybrid simulations versus Cassini MAG data. *grl*, *360*, L04108. doi: 10.1029/2008GL036943

Simon, S., Saur, J., Neubauer, F. M., Wennmacher, A., & Dougherty, M. K. (2011, August). Magnetic signatures of a tenuous atmosphere at Dione. *Geophys. Res. Lett.*, *381*, L15102. doi: 10.1029/2011GL048454

Simon, S., Saur, J., Treeck, S. C., Kriegel, H., & Dougherty, M. K. (2014, May). Discontinuities in the magnetic field near Enceladus. *Geophys. Res. Lett.*, *41*, 3359-3366. doi: 10.1002/2014GL060081

Simon, S., Wennmacher, A., Neubauer, F. M., Bertucci, C. L., Kriegel, H., Saur, J., . . . Dougherty, M. K. (2010, August). Titan's highly dynamic magnetic environment: A systematic survey of Cassini magnetometer observations from flybys TA-T62. *Plantary and Space Science*, *58*, 1230-1251. doi: 10.1016/j.pss.2010.04.021

Smith, H. T., Johnson, R. E., Perry, M. E., Mitchell, D. G., McNutt, R. L., & Young, D. T. (2010, October). Enceladus plume variability and the neutral gas densities in Saturn's magnetosphere. *Journal of Geophysical Research (Space Physics)*, *115*, A10252. doi: 10.1029/2009JA015184

Southwood, D. J., Kivelson, M. G., Walker, R. J., & Slavin, J. A. (1980, November). Io and its plasma environment. *J. Geophys. Res.*, *85*(A11), 5959-5968.

Strobel, D. F. (2005, January). Comparative Planetary Atmospheres of the Galilean Satellites. *Highlights of Astronomy*, *13*, 894.

Strobel, D. F., Saur, J., Feldman, P. D., & McGrath, M. A. (2002). Hubble Space Telecope Space Telescope Imaging Spectrograph search for an atmosphere on Callisto: A Jovian unipolar inductor. *Astrophys. J. Lett.*, *581*, L51-L54.

Strugarek, A., Brun, A. S., Matt, S. P., & Réville, V. (2015, December). Magnetic Games between a Planet and Its Host Star: The Key Role of Topology. *Astrophys. J.*, *815*, 111. doi: 10.1088/0004-637X/815/2/111

Su, Y., Ergun, R., Bagenal, F., & Delamare, P. (2002). Io-related Jovian auroral arcs: Modeling parallel electric fields. *J. Geophys. Res.*, *108*, 1094.

Szalay, J. R., Bonfond, B., Allegrini, F., Bagenal, F., Bolton, S., Clark, G., . . . Wilson, R. J. (2018, November). In Situ Observations Connected to the Io Footprint Tail Aurora. *Journal of Geophysical Research (Planets)*, *123*, 3061-3077. doi: 10.1029/2018JE005752

Tanaka, T., Saito, Y., Yokota, S., Asamura, K., Nishino, M. N., Tsunakawa, H., . . . Terasawa, T. (2009, November). First in situ observation of the Moon-originating ions in the Earth's Magnetosphere by MAP-PACE on SELENE (KAGUYA). *grl*, *36*, L22106. doi: 10.1029/2009GL040682

Tóth, G., Jia, X., Markidis, S., Peng, I. B., Chen, Y., Daldorff, L. K. S., . . . Dorelli, J. C. (2016, February). Extended magnetohydrodynamics with embedded

particle-in-cell simulation of Ganymede's magnetosphere. *Journal of Geophysical Research (Space Physics)*, *121*, 1273-1293. doi: 10.1002/2015JA021997

Turnpenney, S., Nichols, J. D., Wynn, G. A., & Burleigh, M. R. (2018, February). Exoplanet-induced Radio Emission from M Dwarfs. *Astrophys. J.*, *854*, 72. doi: 10.3847/1538-4357/aaa59c

Vasyliūnas, V. M. (2016). Physical origin of pickup currents. *Annales Geophysicae*, *34*(1), 153–156. Retrieved from `https://www.ann-geophys.net/34/153/2016/` doi: 10.5194/angeo-34-153-2016

Vigren, E., Galand, M., Wellbrock, A., Coates, A. J., Cui, J., Edberg, N. J. T., . . . Wahlund, J.-E. (2016, August). Suprathermal Electrons in Titan's Sunlit Ionosphere: Model-Observation Comparisons. *Astrophys. J.*, *826*, 131. doi: 10.3847/0004-637X/826/2/131

Wang, L., Germaschewski, K., Hakim, A., Dong, C., Raeder, J., & Bhattacharjee, A. (2018, April). Electron Physics in 3-D Two-Fluid 10-Moment Modeling of Ganymede's Magnetosphere. *Journal of Geophysical Research (Space Physics)*, *123*, 2815-2830. doi: 10.1002/2017JA024761

Whang, Y. C. (1968, May). Interaction of the Magnetized Solar Wind with the Moon. *Physics of Fluids*, *11*, 969-975. doi: 10.1063/1.1692068

Williams, D. J., Mauk, B. H., McEntire, R. E., Roelof, E. C., Armstrong, T. P., Wilken, B., . . . Lanzerotti, L. J. (1996). Electron beams and ion composition measured at Io and in its torus. *Science*, *274*, 401-403.

Williams, D. J., Mauk, B. H., McEntire, R. E., Roelof, E. C., Armstrong, T. P., Wilken, B., . . . Murphy, N. (1997). Energetic particle signatures at Ganymede: Implications for Ganymede's magnetic field. *Geophys. Res. Lett.*, *24*, 2,163 - 2,166.

Zarka, P. (1998, August). Auroral radio emissions at the outer planets: Observations and theories. *J. Geophys. Res.*, *103*(E9), 20159-20194.

Zarka, P. (2007, April). Plasma interactions of exoplanets with their parent star and associated radio emissions. *Plantary and Space Science*, *55*, 598-617. doi: 10.1016/j.pss.2006.05.045

Zarka, P., Marques, M. S., Louis, C., Ryabov, V. B., Lamy, L., Echer, E., & Cecconi, B. (2018, October). Jupiter radio emission induced by Ganymede and consequences for the radio detection of exoplanets. *Astron. Astrophys.*, *618*, A84. doi: 10.1051/0004-6361/201833586

Zarka, P., Treumann, R. A., Ryabov, B. P., & Ryabov, V. B. (2001). Magnetically-driven planetary radio emissions and applications to extrasolar planets. *Astrophys. Space Sci.*, *277*, 293-300.

Zimmer, C., Khurana, K., & Kivelson, M. (2000). Subsurface oceans on Europa and Callisto: Constraints from Galileo magnetometer observations. *Icarus*, *147*, 329-347.